XXVI ENMC
ENCONTRO NACIONAL DE MODELAGEM COMPUTACIONAL
XIV ECTM
ENCONTRO DE CIÊNCIA E TECNOLOGIA DE MATERIAIS
2023

NAVIER-STOKES/DARCY COUPLING IN CORONARY ARTERY USING GRIDAP LIBRARY

R. M. Lucena[1] - rachel.lucena@eng.uerj.br
H. H. Shin[1] - hshin@pol.una.py
J. Pontes[1] - jose.pontes@eng.uerj.br
N. Mangiavacchi[1] - norberto.mangiavacchi@eng.uerj.br
[1]Universidade do Estado do Rio de Janeiro, Faculdade de Engenharia, Departamento de Engenharia Mecânica – Rio de Janeiro, RJ, Brazil

Abstract. *The use of drug-eluting stents (DES) has become increasingly common in the treatment of coronary artery disease. This procedure involves placing a small metal device, usually coated with a drug-releasing polymer, in a blocked artery to improve blood flow and prevent cardiovascular complications. However, despite the benefits, the increased use of stents has raised concerns, especially regarding the risks of restenosis and thrombosis. The finite element method was used to analyze the flow in a coronary artery, as a first step to study the drug release by the DES. The Navier-Stokes and the Darcy equations were used to model blood flow in a coronary artery considering the arterial lumen and porous arterial wall, thus taking into account the artery characteristics, such as geometry and blood flow. The simulations are performed to find the blood flow through two arterial domains, the wall and the lumen, considering an axi-symmetric two-dimensional geometry. The numerical code was implemented in Julia language using the Gridap library. The contribution of this work is to allow for the analysis of the coupled Navier-Stokes/Darcy problem, which is shown to be important when the arterial wall is not in perfect contact with the stent.*

Keywords: *Drug-eluting stents, Navier-Stokes equation, Darcy's law, Convection-diffusion-reaction equations, Finite element method*

1. INTRODUCTION

Drug-eluting medical devices offer an effective approach for administering drugs within the human body, as they deliver treatment directly to the required location (Zilberman et al., 2010). In line with this notion, drug-eluting stents have gained widespread usage in addressing coronary diseases. A drug-eluting stent (DES) is a small tubular wireframe coated with medication, employed to unclog obstructed coronary arteries. According to Saito & Kobayashi (2021), this approach is the prevailing choice for managing both acute and chronic coronary artery diseases, primarily due to the non-invasive nature of percutaneous coronary intervention.

Numerous investigations encompassing experimental, clinical, and theoretical perspectives, often supported by computational methods, have explored drug delivery, effectiveness, and efficiency of DESs, *e.g.*, Hu et al. (2021); Vo et al. (2018); McGinty et al. (2017); McGinty & Pontrelli (2016); Bozsak et al. (2014); Tzafriri et al. (2012); Stone et al. (2009). It can be verified that the continual enhancement of DES fabrication is needed to mitigate the risks of late thrombotic incidents (Chisari et al., 2016).

In this work, the coupled description of blood flow and plasma filtration is addressed using the Gridap library of Julia programming language. The blood flow in the lumen is represented by the steady-state Navier-Stokes equations, and the plasma filtration through the arterial wall is described by the Darcy equation. The accurate implementation of blood-flow/plasma-filtration is essential in order to solve more complex problems involving the implanted DES.

2. MATHEMATICAL MODEL

Figure 1(a) shows a sketch of the computational domain. It consists of two separated regions: the lumen where the blood is flowing and is denoted by Ω_l, and the arterial wall where the blood plasma is filtrated and is represented by Ω_w. The endothelium Γ_{lw} connects these two regions. Axisymmetric coordinate system with axis direction z and radial direction r is adopted. The radius of the lumen is $r_{lw} = 1.5 \times 10^{-3}$ m, and the thickness of the arterial wall is $r_{\max} - r_{lw} = 0.5 \times 10^{-3}$ m. The length of axis of symmetry is $L_z = 7.0 \times 10^{-3}$ m in the case shown in Fig. 1.

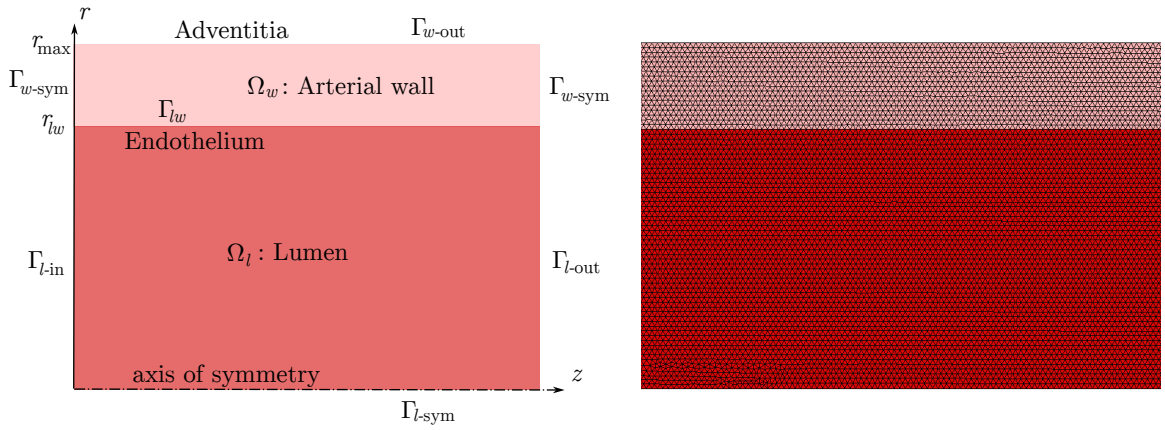

Figure 1: (a) Sketch of the computational domain. (b) Section of the computational mesh employed in numerical simulations.

The blood flow in the lumen is modelled with steady-state incompressible Navier-Stokes equations and the blood is considered as a Newtonian fluid:

$$(\mathbf{u}_l \cdot \nabla)\,\mathbf{u}_l + \frac{1}{\rho}\nabla\, p_l - \nabla \cdot (\nu \nabla \mathbf{u}_l) = 0 \qquad \text{in } \Omega_l, \tag{1}$$

$$\nabla \cdot \mathbf{u}_l = 0 \qquad \text{in } \Omega_l, \tag{2}$$

where $\mathbf{u}_l$ and p_l are the velocity and density-modified pressure of blood in the lumen, and $\nu = \mu_b/\rho$ is the kinematic viscosity of the blood with dynamic viscosity $\mu_b = 3.5 \times 10^{-3}$ Pa·s and density $\rho = 1060$ kg/m^3 (Bozsak et al., 2014).

The filtration of plasma through the arterial wall is described by the Darcy's law with incompressibility constraint as follows:

$$\frac{1}{\kappa}\mathbf{u}_w + \nabla\, p_w = 0 \qquad \text{in } \Omega_w, \tag{3}$$

$$\nabla \cdot \mathbf{u}_w = 0 \qquad \text{in } \Omega_w, \tag{4}$$

where $\mathbf{u}_w$ and p_w are the Darcy velocity and the pressure in the arterial wall, and $\kappa = P_D/\mu_p$ is the hydraulic conductivity per unit of specific weight, with Darcy permeability of the arterial wall given by $P_D = 2 \times 10^{-18}$ m^2 and the dynamic viscosity of plasma by $\mu_p = 7.2 \times 10^{-4}$ Pa·s.

The parabolic velocity profile is prescribed on the lumen inlet boundary, $\Gamma_{l\text{-in}}$, and it is given by

$$\mathbf{u}_{l\text{-in}} = u_{\max}\left[1 - \left(\frac{r}{r_{lw}}\right)^2\right]\hat{z}, \tag{5}$$

where $u_{\max} = 0.33$ m/s is the flow centerline velocity on the axis of symmetry, and $\hat{z}$ is the unit-vector in the direction of z-coordinate. The Reynolds number of the flow is considered

$$\mathrm{Re} = \frac{\rho\, u_{\max}\,(2r_{lw})}{\mu_b} = 300. \tag{6}$$

On the lumen outlet boundary $\Gamma_{l\text{-out}}$, the pressure of $p_{l\text{-out}} = 9.31 \times 10^3$ Pa is prescribed, which is an overpressure compared to the adventitial side. Thus, on the adventitia $\Gamma_{w\text{-out}}$, a null pressure is imposed. On the interface Γ_{lw} between the lumen and the arterial wall, continuity of the pressure and the interface-normal velocity is enforced, *i.e.*,

$$p_l = p_w, \tag{7}$$

$$\mathbf{u}_l \cdot \mathbf{n}_{lw} = \mathbf{u}_w \cdot \mathbf{n}_{lw}, \tag{8}$$

where $\mathbf{n}_{lw}$ is the normal to the interface Γ_{lw}. Finally, no-slip condition for the lumen-side tangential velocity is considered on the interface boundary Γ_{lw}: $\mathbf{u}_l \cdot \mathbf{t}_{lw} = 0$, where $\mathbf{t}_{lw}$ is the tangential to the interface Γ_{lw}.

2.1 Analytical solution

An analytical solution can be found for a simplified one-dimensional axisymmetric equation, where the flow in the direction of axis of symmetry is neglected. Radial distributions of the pressure and velocity in the arterial wall are obtained considering a constant pressure in the endothelium lamina $p_{lw} = p_{l\text{-out}}$. Thus, the analytical solution of the pressure in the arterial wall is

$$p(r) = p_{lw}\left[1 - \frac{\ln\left(r/r_{lw}\right)}{\ln\left(r_{\max}/r_{lw}\right)}\right], \tag{9}$$

and the radial velocity is

$$u_r(r) = \frac{1}{r}\frac{p_{lw}\,\kappa}{\ln\left(r_{\max}/r_{lw}\right)}. \tag{10}$$

In the lumen, considering the constant pressure gradient along the axis of symmetry (z) without the plasma filtration through the arterial wall, the pressure can be expressed as

$$p(z) = p_{l\text{-out}} - \frac{4\mu_b u_{\max}}{r_{lw}}(z - L_z). \tag{11}$$

3. NUMERICAL METHOD

The domain (Fig. 1(a)) composed by the lumen Ω_l and the arterial wall Ω_w are discretized using triangular elements. A section of the triangular mesh of the computational domain is shown in Fig. 1(b).

The weak form of the coupled Navier-Stokes and Darcy equations can be expressed as

$$\begin{aligned}
&\int_{\Omega_l} \left[\left(\mathbf{u}_l \cdot \nabla\right) \mathbf{u}_l\right] \cdot \mathbf{v}_l \, d\Omega + \int_{\Omega_l} \frac{1}{\rho} \left(\nabla p_l\right) \cdot \mathbf{v}_l \, d\Omega + \int_{\Omega_l} \left(\nu \nabla \mathbf{u}_l\right) : \left(\nabla \mathbf{v}_l\right) \, d\Omega + \int_{\Omega_l} \left(\nabla \cdot \mathbf{u}_l\right) q_l \, d\Omega \\
&+ \int_{\Omega_w} \frac{1}{\kappa} \mathbf{u}_w \cdot \mathbf{v}_w \, d\Omega + \int_{\Omega_w} \left(\nabla p_w\right) \cdot \mathbf{v}_w \, d\Omega + \int_{\Omega_w} \left(\nabla \cdot \mathbf{u}_w\right) q_w \, d\Omega \\
&+ \sum_{\Gamma_i^h \in \Gamma_{lw}^h} \alpha_i \int_{\Gamma_i^h} \left(\mathbf{u}_l^+ \cdot \mathbf{n}_{lw}^+ + \mathbf{u}_w^- \cdot \mathbf{n}_{lw}^-\right) \left(\mathbf{v}_l^+ \cdot \mathbf{n}_{lw}^+ + \mathbf{v}_w^- \cdot \mathbf{n}_{lw}^-\right) \, d\Gamma \\
&+ \sum_{\Gamma_i^h \in \Gamma_{lw}^h} \int_{\Gamma_i^h} \left(p_l^+ - p_w^-\right) \left(q_l^+ - q_w^-\right) \, d\Gamma + \sum_{\Gamma_i^h \in \Gamma_{lw}^h} \int_{\Gamma_i^h} \left(\mathbf{u}_l^+ \cdot \mathbf{t}_{lw}^+\right) \left(\mathbf{v}_l^+ \cdot \mathbf{t}_{lw}^+\right) \, d\Gamma = 0, \quad (12)
\end{aligned}$$

where q_l and q_w are the weighting functions belonging to the continuous spaces defined in Ω_l and Ω_w, respectively, $\mathbf{v}_l$ and $\mathbf{v}_w$ are the vector-valued weighting functions belonging to the first order Sobolev spaces with square-integrable first derivative defined in Ω_l and Ω_w, respectively, the superscript $\cdot^+$ corresponds the function-value in the lumen-side of the interface Γ_{lw}, and the superscript $\cdot^-$ corresponds the function-value in the side of arterial wall of the interface Γ_{lw}. The value of penalty parameter α_i is defined as

$$\alpha_i = \frac{\nu}{h_i}, \quad (13)$$

where h_i is the length of the edge (face) Γ_i^h from the set of faces of the boundary triangulation Γ_{lw}^h corresponding to the interface Γ_{lw}. Equation (12) corresponds to the mixed-form of the Galerkin Finite Element Method.

The velocities $\mathbf{u}_l$ and $\mathbf{u}_w$ and the corresponding weighting functions $\mathbf{v}_l$ and $\mathbf{v}_w$ are interpolated by the second degree polynomials and the pressures p_l and p_w with their weighting functions q_l and q_w are interpolated by the linear polynomials. This configuration verifies the LBB condition for the stable numerical solution (Boffi et al., 2013). The integrals are computed using fourth degree quadrature.

Equation (12) is implemented in a finite element framework written in Julia programming language, Gridap library, using two-dimensional axisymmetric coordinates (Badia & Verdugo, 2020; Verdugo & Badia, 2022). The nonlinear system is solved using the Newton method with backtracking line search algorithm implemented in the `LineSearches` packages of Julia (Nocedal & Wright, 2006). For the simulations performed, the default value of norm difference in two successive iterative solutions, which is $\texttt{xtol} = 0.0$, is used, and the infinite norm of residuals for convergence is enforced with $\texttt{ftol} = 10^{-18}$.

4. NUMERICAL EXPERIMENTS

Two sets of numerical experiments are performed. The sketch and the mesh shown in Fig. 1 correspond to the first set, where the flat endothelium is considered flat and is named with a

prefix `flat_`. The other set corresponds to the undulated endothelium, where the endothelium lamina is displaced in the radial direction using the following function:

$$r(z) = r_{lw}\left[1 - A\left(\frac{1}{2} + \frac{1}{2}\cos\frac{2\pi(z - z_0)}{L_z}\right)^{12}\right], \tag{14}$$

where $A = 0.5$ is the maximum radial displacement of the endothelium from the flat cases, $L_z = 15.0 \times 10^{-3}$ m is the length of the computational domain, and $z_0 = 3.5 \times 10^{-3}$ m is the position of the trough position of the undulated endothelium. These cases are named with a prefix `und_`. Table 1 shows the both sets of numerical experiments performed with the information of mesh size (h), numbers of nodes and cells (elements) for each mesh.

Table 1: Computational mesh employed in simulations.

Mesh ID	mesh size (h)	# nodes	# cells	Mesh ID	mesh size (h)	# nodes	# cells
`flat_01`	2.0×10^{-4}	209	358	`und_01`	2.0×10^{-4}	431	752
`flat_02`	1.0×10^{-4}	738	1,358	`und_02`	1.0×10^{-4}	1,552	2,886
`flat_03`	5.2×10^{-5}	2,713	5,196	`und_03`	5.2×10^{-5}	5,825	11,220
`flat_04`	2.6×10^{-5}	10,490	20,526	`und_04`	2.6×10^{-5}	22,492	44,130
`flat_05`	1.3×10^{-5}	41,084	81,266	`und_05`	1.3×10^{-5}	88,106	174,510

5. NUMERICAL RESULTS

The volume fluxes can be employed as a verification and estimate of the approximation errors. This computation is also equivalent to estimate the error in the divergence free constraint of the velocity field. In the lumen, the inlet volume flux on $\Gamma_{l\text{-in}}$ is balanced by the sum of the fluxes on $\Gamma_{l\text{-out}}$ and the plasma filtered on the interface Γ_{lw}. Thus, the error in net flux of the lumen is

$$\texttt{error\_flux}^h(\Omega_l) = \left| \int_{\Gamma^h_{l\text{-in}}} \mathbf{n}\cdot\mathbf{u}_l \, d\Gamma + \int_{\Gamma^h_{l\text{-out}}} \mathbf{n}\cdot\mathbf{u}_l \, d\Gamma + \int_{\Gamma^h_{lw}} \mathbf{n}\cdot\mathbf{u}_l \, d\Gamma \right|, \tag{15}$$

where $|\cdot|$ is the absolute value operator and the superscript h indicates the mesh size. In the arterial wall, the flux filtered on Γ_{lw} equals the flux on adventitia boundary $\Gamma_{w\text{-out}}$

$$\texttt{error\_flux}^h(\Omega_w) = \left| \int_{\Gamma^h_{lw}} \mathbf{n}\cdot\mathbf{u}_w \, d\Gamma + \int_{\Gamma^h_{w\text{-out}}} \mathbf{n}\cdot\mathbf{u}_w \, d\Gamma \right|. \tag{16}$$

Finally, the net flux considering the whole domain is:

$$\texttt{error\_flux}^h(\Omega) = \left| \int_{\Gamma^h_{l\text{-in}}} \mathbf{n}\cdot\mathbf{u}_l \, d\Gamma + \int_{\Gamma^h_{l\text{-out}}} \mathbf{n}\cdot\mathbf{u}_l \, d\Gamma + \int_{\Gamma^h_{w\text{-out}}} \mathbf{n}\cdot\mathbf{u}_w \, d\Gamma \right|. \tag{17}$$

The results obtained for the error net flux in the lumen, arterial wall and the whole domain are shown in Fig. 2 for both cases considered. Each data point on the curves corresponds to a specific mesh size, as detailed in Table 1.

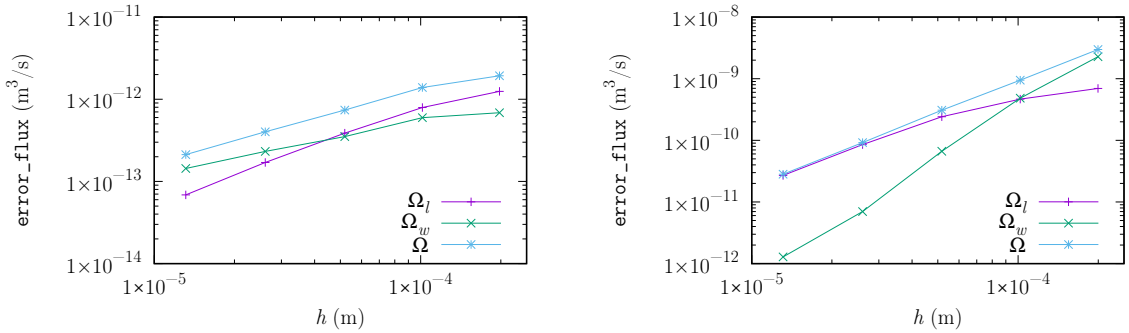

Figure 2: Error in the net volume flux: (a) flat endothelium, (b) undulated endothelium.

An estimate of the asymptotic order of convergence is given by:

$$N = -\frac{\log\left(\texttt{error\_flux}^{h_f}/\texttt{error\_flux}^{h_c}\right)}{\log\left(h_f/h_c\right)}, \tag{18}$$

where h_f and h_c are the finer and coarser mesh sizes, respectively. This estimate N is the measure of the slops in Fig. 2: $N \approx 0.9$ for the flat endothelium, and $N \approx 1.7$ for the undulated endothelium simulations.

The analytical solutions in the arterial wall, Eqs. (9) and (10), and the results obtained from the numerical simulations for flat endothelium (case `flat_05`) are in good agreement as can be seen in Fig. 3. Small discrepancies are observed near the boundaries (Γ_{lw} and $\Gamma_{w\text{-out}}$) due to the limitations of the imposed boundary conditions in the numerical simulation and the simplifications assumed for the analytical solution.

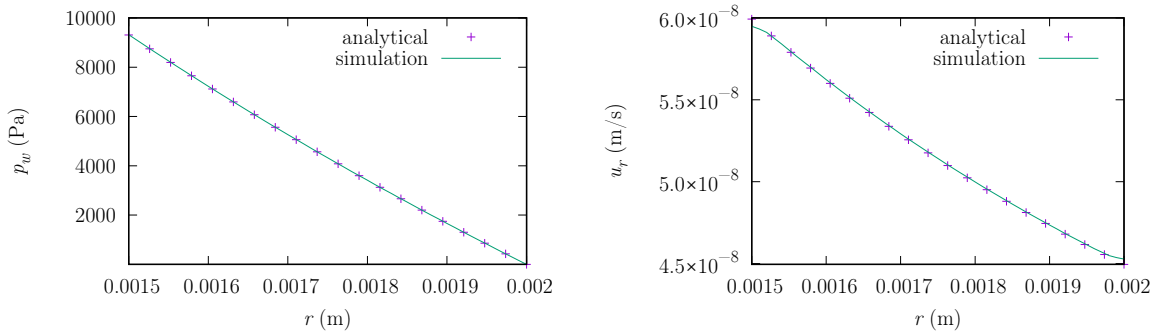

Figure 3: Comparison between the results from the simulation in the arterial wall and the simplified analytical solution: (a) pressure and (b) radial velocity.

Figure (4) shows the pressure in the lumen obtained from the numerical simulation (case `flat_05`) compared to the analytical solution presented in Eq. (11). The comparison shows that the numerical results have a satisfactory agreement with the analytical solution, considering that the later is obtained assuming that the plasma filtration flow rate across the wall is negligible.

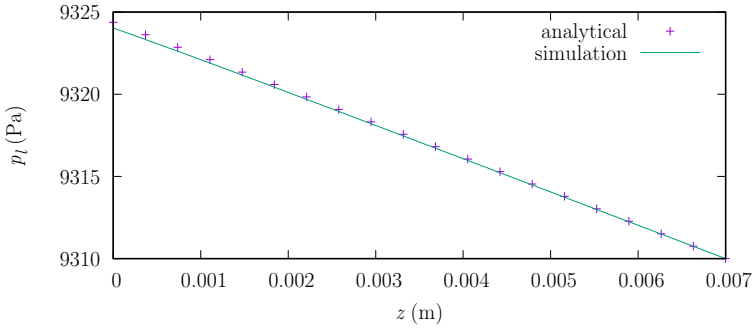

Figure 4: Comparison between the pressure in the lumen obtained from the simulation and the simplified analytical solution.

The results shown in Figs. 2-5 serve as a verification of the correctness of the computational implementation. The developed code was then applied to simulate a partial arterial occlusion. The analysed geometry represents a coronary artery with an axisymmetric 75% area occlusion.

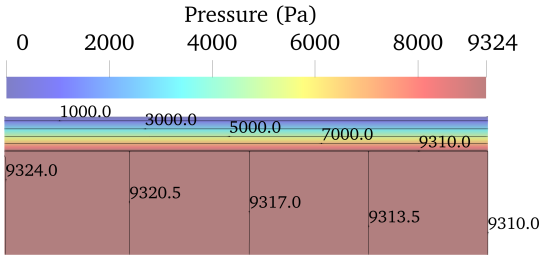

Figure 5: Pressure distribution with contour lines for flat endothelium (case `flat_05`).

Similarly to the flat endothelium case, the pressure distribution in the undulated endothelium shows a large pressure gradient across the arterial wall, and a small gradient on the lumen in the axial direction (see Fig. 6). However, the undulated case shows a localised region of a higher pressure gradient in the throat, associated to the higher velocity and larger head loss in this region (see Fig. 7). On one hand, the pressure drops in the throat region, and the there is a gradual pressure recovery up to the outflow boundary. On the other hand, there is a much larger head loss in the undulated endothelium case.

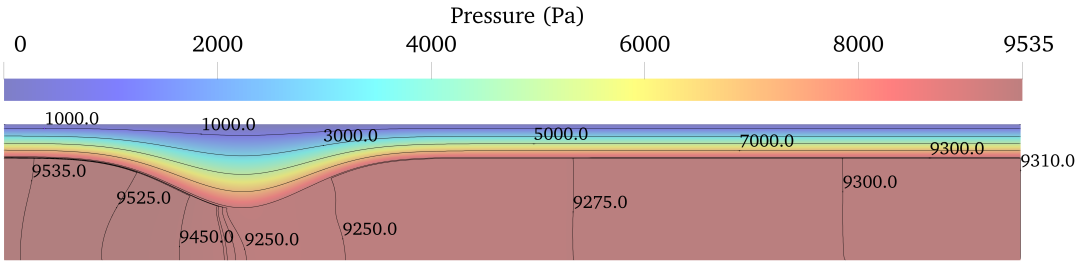

Figure 6: Pressure distribution with contour lines for undulated endothelium (case `und_05`).

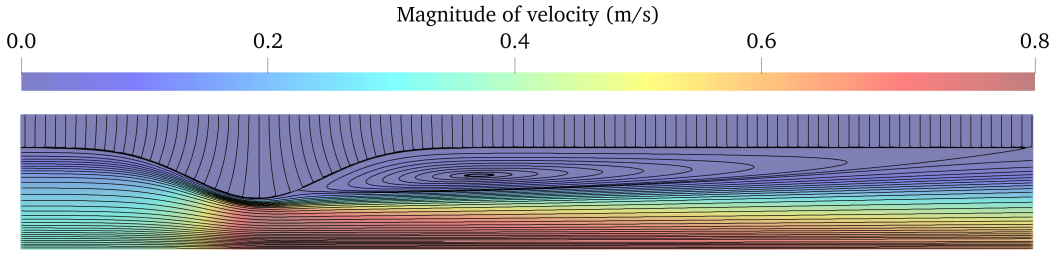

Figure 7: Velocity distribution with streamlines for undulated endothelium (case `und_05`).

6. CONCLUSIONS

A computational model for the simulation of blood flow in the arterial lumen and plasma filtration in the arterial wall was developed and verified by comparison with simplified analytical solutions. The flow in the lumen is modelled by the Navier-Stokes equations, and the plasma filtration in the wall is modelled by Darcy's law. The discrete equations for the two domains are obtained by the mixed Galerkin Finite Element method, using LBB-complying triangular elements, and the two domain solutions are coupled using a penalty methods. The implementation was performed using the Julia programming language and the Gridap library.

The combination of these techniques will be used to accurately model the interaction between the stent and the artery in future works, providing important information about the effects of stent position, size, and geometry on the drug transport. Additionally, the finite element modelling and flow and transport equations can be used to simulate different clinical scenarios, allowing for better stent parameter selection, based on patient data, and the development of new stent designs.

Acknowledgements

The authors would like to acknowledge financial support from FAPERJ, CAPES and CNPq.

REFERENCES

Badia, S., & Verdugo, F. (2020). Gridap: An extensible finite element toolbox in Julia. *Journal of Open Source Software*, *5*(52), 2520.

Boffi, D., Brezzi, F., & Fortin, M. (2013). *Mixed finite element methods and applications*, vol. 44. Springer.

Bozsak, F., Chomaz, J., & Barakat, A. (2014). Modelling the transport drugs of eluted from stents: physical phenomena driving drug distribution in the arterial wall. *Biomech Model Mechanobiol*, *13*, 327–347.

Chisari, A., Pistritto, A., Piccolo, R., Manna, A. L., & Danzi, G. (2016). The ultimaster biodegradable-polymer sirolimus-eluting stent: An updated review of clinical evidence. *Int. J. Mol. Sci.*, *17(9)*, 1490.

Hu, S., Li, Z., Shen, D., Zhu, D., Huang, K., Su, T., Dinh, P.-U., Cores, J., & Cheng, K. (2021). Exosome-eluting stents for vascular healing after ischaemic injury. *Nature biomedical engineering*, (pp. 1–15).

McGinty, S., King, D., & Pontrelli, G. (2017). Mathematical modelling of variable porosity coatings for controlled drug release. *Medical engineering & physics*, *45*, 51–60.

McGinty, S., & Pontrelli, G. (2016). On the role of specific drug binding in modelling arterial eluting stents. *J Math Chem*, *54*, 967–976.

Nocedal, J., & Wright, S. J. (2006). *Numerical optimization*. Springer New York, NY.

Saito, Y., & Kobayashi, Y. (2021). Contemporary coronary drug-eluting and coated stents: A mini-review. *Cardiovascular intervention and therapeutics*, *36*(1), 20–22.

Stone, G. W., Lansky, A. J., Pocock, S. J., Gersh, B. J., Dangas, G., Wong, S. C., Witzenbichler, B., Guagliumi, G., Peruga, J. Z., Brodie, B. R., et al. (2009). Paclitaxel-eluting stents versus bare-metal stents in acute myocardial infarction. *New England Journal of Medicine*, *360*(19), 1946–1959.

Tzafriri, A. R., Groothuis, A., Price, G. S., & Edelman, E. R. (2012). Stent elution rate determines drug deposition and receptor-mediated effects. *Journal of Controlled Release*, *161*(3), 918–926.

Verdugo, F., & Badia, S. (2022). The software design of Gridap: A finite element package based on the Julia JIT compiler. *Computer Physics Communications*, *276*, 108341.

Vo, T. T., Morgan, S., McCormick, C., McGinty, S., McKee, S., & Meere, M. (2018). Modelling drug release from polymer-free coronary stents with microporous surfaces. *International Journal of Pharmaceutics*, *544*(2), 392–401.

Zilberman, M., Kraitzer, A., Grinberg, O., & Elsner, J. J. (2010). Drug-eluting medical implants. *Drug Delivery*, (pp. 299–341).